WISC

UNIVERSITY OF WISCONSIN • MADISON, WISCONSIN

PLASMA PHYSICS

45
2-8-96 JS (2)

LOWER HYBRID ACCESSIBILITY IN A LARGE, HOT REVERSED FIELD PINCH

R.A. Dziubek, R.W. Harvey†, S.A. Hokin, and E. Uchimoto‡

DOE/ER/53212-269 November 1995

ONSIN

NOTICE

Printed in the United States of America
Available from
National Technical Information Service
U.S. Department of Commerce
5285 Port Royal Road
Springfield, VA 22161

NTIS Price codes
Printed copy: A03
Microfiche copy: A01

Lower Hybrid Accessibility in a Large, Hot Reversed Field Pinch

R.A. Dziubek, R.W. Harvey†, S.A. Hokin, and E. Uchimoto‡

Department of Physics, University of Wisconsin, Madison, Wisconsin 53706
United States of America

ABSTRACT

Accessibility and damping of the slow wave in a reversed field pinch (RFP) plasma is investigated theoretically, using projected Reversed Field Experiment (RFX) plasma parameters. By numerically solving the hot plasma dispersion relation, regions of propagation are found and the possibility of mode conversion is analyzed. If the parallel index of refraction of the wave is chosen judiciously at the edge of the plasma, the slow wave is accessible to a target region located just inside the reversal surface without mode conversion. Landau damping is also optimized in this region. A representative fast electron population is then added in order to determine its effect on accessibility and damping. The presence of these electrons, whose parameters were estimated by extrapolation of Madison Symmetric Torus (MST) data, does not affect the accessibility of the wave. However, the initial phase velocity of the wave needs to be increased somewhat in order to maintain optimal damping in the target zone.

† Permanent address: General Atomics, San Diego, California 92186 USA

‡ Permanent address: Department of Physics and Astronomy, University of Montana, Missoula, Montana 59812 USA

I. Introduction

Reversed field pinch (RFP) plasmas are characterized by comparable toroidal and poloidal magnetic field components ($B_\phi \approx B_\theta$) where both elements of the field are powered by a poloidal field circuit driving a toroidal current. Poloidal current is partly driven by the dynamo mechanism which is theorized to be caused by the interaction of fluctuations in fluid flow velocity and magnetic field [1]. Unfortunately, the effects of the dynamo extend beyond current generation to include mode locking, turbulence generation, and enhanced particle and energy transport [2,3,4]. Control of the dynamo, then, is critical to the improvement of an RFP.

Recent experiments suggest that dynamo activity can be suppressed by externally driving a poloidal current in the plasma [5,6]. In the search for a form of steady state current drive, Shiina, *et al.* [7] and Ishii, *et al.* [8] performed theoretical investigations of current drive for the TPE-RX project using the fast magnetosonic wave ($\omega_{ci} < \omega < \omega_{LH}$, where ω_{ci} is the ion cyclotron frequency and ω_{LH} is the lower hybrid frequency). They favor the fast wave over the slow wave because of its high parallel phase velocity, which is predicted to allow the wave to reach the interior of a high beta RFP plasma. Their calculations show that the fast wave is an efficient current driver in the high-density regions of the plasma and a strong candidate for creating a dynamo-free RFP.

Unlike the fast wave, the slow wave possesses the advantages of a higher frequency and a simpler antenna design. While accessibility to the core may be limited, investigation by Uchimoto, *et al.* [9], using the cold and warm plasma dispersion relations and an RFP-adapted version of the Brambilla ray-tracing code [10] showed that the wave can get deep enough into the plasma to reach a target region at $r/a \approx 0.70$. According to numerical simulations run with the three dimensional resistive MHD code, DEBS [11], currents added to this

region stabilize a larger portion of the plasma than if current were added at other radii. This makes the slow wave an attractive option.

This paper extends these previous investigations of lower hybrid wave accessibility in an RFP in two directions. First, it is a theoretical exploration of the accessibility of a high frequency slow wave ($f \approx$ 1.0-1.5 GHz) launched into the projected plasma of the Reversed Field Experiment (RFX) RFP [12] at 2 MA plasma current. This machine is characterized by larger dimensions (R = 2.0 m, a = 0.457 m) and a larger maximum current (I < 2 MA) than other machines. It should be noted that RFX has not actually achieved a 2 MA current to date. However, for the purpose of examining this subject at higher temperatures, we have extrapolated the present performance of the Madison Symmetric Torus (MST) [13] and RFX up to this current. RFX will run with a magnetic field strength of 8.75 kG at 2 MA, placing the lower hybrid frequency at about 0.57 GHz. In order to avoid strong ion plasma resonances, a frequency of 2.0 to 2.5 times the lower hybrid frequency was chosen. Hokin, *et al.* [14], have investigated the feasibility of using lower hybrid current drive in a 2 MA RFX in order to maintain 10% beta. In the course of their work, they projected plasma parameters for a density scan of RFX which will also be used for this work and are reproduced in Table I.

Secondly, this paper investigates the effect of a small fast electron population on accessibility and damping. RFP's have a 2-20% fast electron population near the edge of the plasma [15,16]. Since these electrons change the edge temperature of the plasma, they are expected to alter the position of Landau damping of the wave. By adapting the dispersion code to include this population, their impact is analyzed.

The paper is organized as follows: Section II describes the hot plasma dispersion relation used and lists assumptions made about the electron and ion

species in RFX. In Section III, initial accessibility studies for an electron/ion plasma are performed. The method used to find regions of optimal Landau damping is covered in Section IV. The addition of a fast electron species is discussed in Section V. Section VI is a short conclusion.

II. The Hot Plasma Dispersion Relation

In order to explore the accessibility conditions of the lower hybrid wave, the hot plasma dispersion relation described by Swanson [17] is used. This dispersion relation is derived assuming a drifting, anisotropic Maxwellian distribution of particles. By rotating the local Cartesian coordinate system so that the wave lies in the planes parallel and perpendicular to the magnetic field, Swanson's dispersion relation can be simplified to

$$\left[\gamma\left(\gamma-K_0+n_\perp^2\right)+K_2^2\right]K_3+n_\perp^2\left[\left(\gamma-K_0+n_\perp^2\right)K_1-K_2^2\right]+ K_4\left(\gamma-K_0+n_\perp^2\right)\left(2n_\perp n_{//}+K_4\right)-K_5\left[\gamma K_5+2K_2\left(n_\perp n_{//}+K_4\right)\right]=0 \quad (1)$$

where $\gamma = n_{//}^2 - K_1$ and the six tensor coefficients are expressed below:

$$K_0 = 2\sum_j \frac{\omega_{pj}^2 c e^{-\lambda_j}}{\omega^2 n_{//} v_{t//j}} \sum_{n=-\infty}^{\infty} \lambda_j \left(I_n - I_n'\right) \times\left[\left(1-\frac{n_{//}v_{0j}}{c}\right)Z\left(\zeta_{nj}\right)+\frac{n_{//}v_{t//j}}{c}\left(1-\frac{T_{\perp j}}{T_{//j}}\right)\frac{Z'\left(\zeta_{nj}\right)}{2}\right] \quad (2)$$

$$K_1 = 1+\sum_j \frac{\omega_{pj}^2 c e^{-\lambda_j}}{\omega^2 n_{//} v_{t//j}} \sum_{n=-\infty}^{\infty} \frac{n^2 I_n}{\lambda_j} \times\left[\left(1-\frac{n_{//}v_{0j}}{c}\right)Z\left(\zeta_{nj}\right)+\frac{n_{//}v_{t//j}}{c}\left(1-\frac{T_{\perp j}}{T_{//j}}\right)\frac{Z'\left(\zeta_{nj}\right)}{2}\right] \quad (3)$$

$$K_2 = i\sum_j \frac{\varepsilon_j \omega_{pj}^2 c e^{-\lambda_j}}{\omega^2 n_{||} v_{t||j}} \sum_{n=-\infty}^{\infty} n(I_n - I_n') \times\left[\left(1-\frac{n_{||}v_{0j}}{c}\right)Z(\zeta_{nj})+\frac{n_{||}v_{t||j}}{c}\left(1-\frac{T_{\perp j}}{T_{||j}}\right)\frac{Z'(\zeta_{nj})}{2}\right] \quad (4)$$

$$K_3 = 1-\sum_j \frac{\omega_{pj}^2 c^2 e^{-\lambda_j}}{\omega^3 n_{||}^2 v_{t||j}^2} \sum_{n=-\infty}^{\infty} I_n(\omega + n\omega_{cj}) \times\left\{\frac{2n\omega_{cj}T_{||j}v_{0j}}{\omega T_{\perp j} v_{t||j}} Z(\zeta_{nj})+\left[1+\frac{n\omega_{cj}}{\omega}\left(1-\frac{T_{||j}}{T_{\perp j}}\right)\right]Z'(\zeta_{nj})\right\} \quad (5)$$

$$K_4 = \sum_j \frac{n_\perp \omega_{pj}^2 e^{-\lambda_j}}{n_{||}\omega\omega_{cj}} \sum_{n=-\infty}^{\infty} \frac{n I_n}{\lambda_j} \times\left\{\frac{n\omega_{cj}v_{0j}}{\omega v_{t||j}} Z(\zeta_{nj})+\left[\frac{T_{\perp j}}{T_{||j}}-\frac{n\omega_{cj}}{\omega}\left(1-\frac{T_{\perp j}}{T_{||j}}\right)\right]\frac{Z'(\zeta_{nj})}{2}\right\} \quad (6)$$

$$K_5 = i\sum_j \frac{n_\perp \varepsilon_j \omega_{pj}^2 e^{-\lambda_j}}{n_{||}\omega\omega_{cj}} \sum_{n=-\infty}^{\infty} (I_n - I_n') \times\left\{\frac{n\omega_{cj}v_{0j}}{\omega v_{t||j}} Z(\zeta_{nj})+\left[\frac{T_{\perp j}}{T_{||j}}-\frac{n\omega_{cj}}{\omega}\left(1-\frac{T_{\perp j}}{T_{||j}}\right)\right]\frac{Z'(\zeta_{nj})}{2}\right\} \quad (7)$$

In the above expressions, the summation over j is a summation over species, ω_{pj} are the plasma frequencies, ω_{cj} are the cyclotron frequencies, and ω is the wave frequency. The $n_{||}$ and $n_\perp$ are the parallel and perpendicular indices of refraction of the wave and c is the speed of light in a vacuum. The longitudinal thermal velocity of each species is represented by $v_{t||j}$ and the drift velocity by v_{0j}. The λ_j are Larmor radius length scales equal to $(1/2)k_\perp^2\rho_{Lj}^2$, where ρ_{Lj} is the Larmor radius of the species. I_n and I_n' are the modified Bessel function of the *nth* order and its derivative, where the argument for each is λ_j. Z and Z' are the Fried-Conte dispersion function and its derivative with the argument $\zeta_{nj} = \left(\omega + n\omega_{cj} - k_z v_{0j}\right)/k_z v_{t||j}$. The sign of the charge of each species is represented by ε_j.

Several assumptions were made about the electron and ion distributions of RFX. Ions were taken to be protons. Quasineutrality was upheld by setting $n_e = n_i$, where n_j represents number density. The ion and electron temperatures were set equal to each other since these two species are assumed to be collisionally coupled in RFX at 2 MA. The parallel and perpendicular temperatures of each species were also set equal. Lastly, it was assumed that neither species has a significant drift velocity so that v_0 could be set to zero. For the majority of the investigation covered in this paper, the projected temperature and density of RFX at $I/N = 6\times10^{-14}\ A\cdot m$ were used as plasma parameters. In the code, the density profile is parabolic: $n_j = n_{j0}[1-(r/a)^2]$. A quartic temperature profile is assumed for each species: $T_j = T_{j0}[1-(r/a)^4]$.

The dispersion code assumes an infinite slab of plasma with a fixed temperature and density. A wave of fixed frequency and parallel index of refraction is given and the code determines the perpendicular index of refraction using rootsolving methods. The plasma temperature and density and wave parallel index of refraction are then changed to correspond to a radial step by the wave deeper into the plasma and the next root is found. This method allows effects such as cutoff, mode conversion, and optimization of Landau damping to be explored. It is also possible to use this process to observe the effects of fast electrons, which make up 10 - 20% of the edge electron density in an RFP [15,16].

III. Accessibility in an Electron-Ion Plasma

When considering wave accessibility, one is looking for points in the plasma which are resonances or cutoffs for the wave. Since $n_{//}$ is set at each step of the plasma, we are looking for places where $n_\perp$ passes through infinity

or zero. It is expected that the wave should become resonant with the ion plasma frequency at $r/a \approx 0.65$ and, depending upon the value of $n_{//}$, with the electron parallel thermal velocity at deeper points in the plasma. The first of these points is a weak resonance and does not impede the travel of the wave. The second is a region of strong Landau damping in the center of the electron velocity distribution function. Cutoff can be determined by examining the cold plasma dispersion relation. By using the determinant of the dispersion relation and requiring that $\omega = 2\omega_{LH} = 2\sqrt{\omega_{ce}\omega_{ci}}$ (recall that, as density becomes high, $\omega_{LH} \rightarrow \sqrt{\omega_{ce}\omega_{ci}}$), an approximate expression for the requirement on $n_{//}$ may be generated:

$$n_{//} \geq \left(1+\omega_{pe}^2/\omega_{ce}^2\right)^{1/2} + \omega_{pe}/\omega_{ce} \qquad (8)$$

In general, this limits the travel of the wave in certain high density regions of the plasma.

In the case of RFX, the cutoff can be seen by plotting the contours of $n_\perp^2 = 0$ on a diagram of $n_{//}$ and density. Figure (1) shows that the cutoff follows that predicted by Eq. (8) fairly closely. The region of resonance between the wave and the thermal electrons is also indicated with a dashed line. By assuming that $n_{//}$ increases as the wave steps into the plasma according to $n_{//} = n_{//edge}/(r/a)$, the exact path of the wave through the plasma may be traced. Laying this trajectory onto the map of the cutoffs, it is possible to observe the position of the wave relative to the cutoff. One great concern when using the slow wave is that of mode conversion to the fast wave. Figure (2) displays $n_\perp^2$ as a function of density for selected values of $n_{//}$. Note the extra path at the mode conversion density. This is an evanescent mode inside the cutoff. From this

figure, it can be concluded that mode conversion does not represent a threat to slow wave propagation if $n_{\parallel edge} > 5.0$.

IV. Landau Damping Efficiency

A second criterion in considering the feasibility of lower hybrid current drive in an RFP is that edge conditions optimize electron Landau damping within the area of interest in the plasma. Prior analysis by Uchimoto, *et al.* [9] used the warm plasma dielectric tensor to determine that Landau damping is optimized in those regions characterized by $v_{ph}/v_{tle} \approx 2.5$ where v_{ph} is the parallel phase velocity of the wave and may be expressed as $v_{ph} = c/n_{\parallel}$. Damping can be analyzed [18] by plotting v_{ph}/v_{tle} as a function of temperature and $n_{\parallel}$ (Fig. (3)). Regions of $v_{ph}/v_{tle} < 2.0$ are characterized by excessive damping while regions of $v_{ph}/v_{tle} > 3.0$ are regions of little damping. Assuming that $n_{\parallel}$ varies as described earlier, it is possible to invoke the "ray-tracing" technique employed in Fig. (1) to overlay the path of the wave onto the plot of v_{ph}/v_{tle} contours. By adjusting the starting value of $n_{\parallel}$, the wave can be made to propagate through the outer region of the plasma with little damping until it reaches the region where current drive is desired.

A more quantitative method of determining the region of optimal Landau damping can be found by adapting a technique suggested by Stix [19]. He determines the damping rate, $\Gamma = P/W$, where P is the power per unit volume deposited into the plasma and W is the wave energy density. Power can be expressed as

$$P = -\frac{i\omega}{16\pi} \boldsymbol{E}^* \cdot \underline{\underline{\boldsymbol{K}}} \cdot \boldsymbol{E} + complex \;\; conjugate \qquad (9)$$

where $\boldsymbol{E}$ is the complex amplitude of the wave electric field and $\underline{\underline{\boldsymbol{K}}}$ is the hot plasma dielectric tensor. From cold plasma theory, the polarization of the slow wave is such that $|E_x| >> |E_z|$ and $|E_x| >> |E_y|$, so that $\boldsymbol{E}$ is almost parallel to $\boldsymbol{k}$ and E_y can be effectively ignored. Then,

$$P = -\frac{i\omega}{8\pi}\left[i|E_x|^2 Im(K_1) + 2i\,Re(E_x E_z^*) Im(K_4) + i|E_z|^2 Im(K_3)\right] \tag{10}$$

in which the term dependent on $|E_z|^2$ is power deposited by Landau damping, the term dependent on $|E_x|^2$ is power deposited by transit time magnetic pumping, and the term dependent on $E_x E_z^*$ is a cross term.

The wave energy is, from classical electromagnetic theory,

$$W = \frac{1}{16\pi}\left[\boldsymbol{B}^* \cdot \boldsymbol{B} + \boldsymbol{E}^* \cdot \frac{\partial}{\partial\omega}\left(\omega \underline{\underline{\boldsymbol{K}}}_h\right) \cdot \boldsymbol{E}\right] \tag{11}$$

where $\boldsymbol{B}$ indicates the wave magnetic field and $\underline{\underline{\boldsymbol{K}}}_h$ is the hermitian conjugate of the dielectric tensor. Since the slow wave is predominantly electrostatic, $\boldsymbol{B} \approx 0$, and the equation reduces to

$$W = \frac{1}{16\pi}\left[|E_x|^2 \frac{\partial}{\partial\omega}\left(\omega K_1^*\right) + 2Re(E_x E_z^*) \frac{\partial}{\partial\omega}\left(\omega K_4^*\right) + |E_z|^2 \frac{\partial}{\partial\omega}\left(\omega K_3^*\right)\right]. \tag{12}$$

Using the electron elements of the dielectric tensor in the power equation, the electron Landau damping rate is then the Landau damping term of the power equation divided by the total wave energy. The relative value of E_x is of use here and may be determined from the *y*- and *z*-components of the wave equation:

$$\frac{E_x}{E_z} = -\frac{\left[K_5^2 + \left(K_1 + K_0 - n^2\right)\left(K_3 - n_\perp^2\right)\right]}{\left[K_2 K_5 + \left(K_1 + K_0 - n^2\right)\left(K_4 + n_\perp n_{//}\right)\right]}. \tag{13}$$

By applying Eqs. (10), (12), and (13) to the definition of Γ, we get the following expression for the Landau damping rate:

$$\Gamma_{LD} \approx 2\omega\left[\frac{Im(K_3)}{\left|E_x/E_z\right|^2 K_1^* + 2Re(E_x/E_z)K_4^* + K_3^*}\right]. \tag{14}$$

Because we have been working in a slab geometry thus far, we cannot maximize the Landau damping rate by taking the derivative with respect to the flux surface area, $d\Gamma_{LD}/d\sigma$. However, it is possible to analytically estimate the region of ideal damping. In order for damping to be ideal, the damping rate must be comparable to the inverse of the desired time of damping:

$$\Gamma_{LD}\Delta t \approx O(1) \tag{15}$$

It is not unreasonable to expect the wave to damp out within one poloidal revolution at $r/a \approx 0.70$, so that

$$\Delta t = \frac{l}{v_{g//}} = \frac{2\pi r}{c/n_{//}} \tag{16}$$

In the above expression, l is the damping path length and $v_{g//}$ is the group velocity of the wave in the parallel direction which we have approximated as the parallel phase velocity. By allowing the ideal Landau damping rate to equal the inverse of Δt and plotting that curve over a graph of the curve determined by Eq. (14), the location of optimal damping may be found. Figure (4) shows the

results of applying this logic to RFX for $n_{\|edge} = 4.5$ to $n_{\|edge} = 6.0$. The region of optimal Landau damping lies at the intersection of the curves representing Γ_{LD} and Δt. Within the accuracy of our order-of-magnitude calculations, it can be seen that $n_{\|edge}$ between 4.5 and 5.5 will allow for proper damping at $r/a \approx 0.70$.

In order to test the validity of this prediction, the data for the case of $I/N = 6\times10^{-14}\,A/m$ with $n_{\|edge} = 5.5$ were entered into the RFP-adapted version of the Brambilla ray-tracing program [10]. Results are shown in Fig. (5). The ray enters the plasma at the outboard edge and proceeds around the poloidal plane of the torus until it is completely damped. The power deposition profile (Fig. (6)) shows a sharp spike at $r/a \approx 0.70$, indicating that current was driven in the desired region. With the frequency chosen at $f \approx 2f_{LH}$ to avoid ion plasma resonances, all of the wave power was delivered to the electrons.

Additional simulations were run with different starting values for the parallel index of refraction. Figures (7) and (8) show the results of those cases. Most notable are the case for $n_{\|edge} = 2.4$, in which the wave is evanescent and $n_{\|edge} = 2.6$, in which the wave is a surface mode. These effects occur because of the proximity of the cutoff. When $n_{\|edge} = 4.0$, the wave starts out with a higher phase velocity than if $n_{\|edge} = 5.5$ and takes longer to match velocities with the electrons. Therefore, it goes deeper into the plasma before damping. On the other hand, if $n_{\|edge} = 8.0$, the wave starts out slower than if $n_{\|edge} = 5.5$ and interacts with electrons further from the core. Table I shows the optimum values of $n_{\|edge}$ for a full density scan of RFX at 2 MA.

V. Fast Electron Effects

One special concern regarding lower hybrid current drive in an RFP involves the larger density of high velocity electrons than would be seen in a

tokamak. Measurements on a variety of RFP devices show that superthermal electrons make up 2-20% of the edge electron population. [15,16] In MST, Stoneking determined that fast electrons carry nearly all the edge poloidal current, have a parallel temperature comparable to the central electron temperature, and a perpendicular temperature roughly equal to the edge bulk electron temperature [16]. Other groups have reported similar results.

RFX is expected to have fast electron energies in the keV range. [15,20] The fast electrons are nearly collisionless within the plasma and so may be thought of as a separate species from the bulk electrons. Adapting the hot plasma code to accommodate the fast electrons involves adding those electrons to the sum over species in each of the *K*-terms of the dielectric tensor (Eqs. (2)-(7)). As mentioned above, the parallel temperature of the fast electrons is about equal to the central electron temperature, so it can be assumed that it remains constant across the minor radius of the plasma. The fast electron drift velocity was determined by setting $J = en_h v_{oh}$, where J is a model current density profile, n_h is the hot electron density, and v_{oh} is the drift velocity of the hot electrons. We assume $n_h/n_e = 10\%$. The perpendicular temperature of the fast electrons was set equal to the edge bulk electron temperature.

Because the position of the cutoff is, in theory, only dependent upon the local density and magnetic field, the addition of fast electrons is not expected to affect it. On the other hand, the position of the thermal resonance is strongly temperature dependent and should shift further from the core as the effective temperature at the outer radii increases. The shift is not severe enough to limit accessibility, however, as can be seen in Fig. (9).

With the wave encountering a different distribution of electrons in the outer regions of the plasma, Landau damping should be influenced. The

presence of the fast electrons in any region near the edge of the plasma effectively increases the temperature in that region, so that the area of optimal damping moves further out to the edge. By using the analytical methods presented in Section IV, the exact effects of this species can be analyzed. The intersection of the curves for Γ_{LD} and Δt have moved to higher r/a for each $n_{\parallel edge}$ and the spectrum has widened (Fig. (10)). This would indicate that the fast electrons have indeed made the edge of the plasma hotter and also broadened the velocity distribution in this region. Consequently, the wave must be launched with a somewhat faster parallel phase velocity at the edge of the plasma in order to maintain ideal damping.

VI. Conclusions

In conclusion, the slow wave was found to be accessible to $r/a \approx 0.70$ in an RFP for edge parallel indices of refraction which meet the derived criteria (Eq. (8)). There is a weak ion plasma resonance at $r/a \approx 0.65$ and a strong electron thermal resonance at deeper points in the plasma. This thermal resonance marks a region of powerful Landau damping in the center of the electron velocity distribution. Mode conversion can be expected in high density regions of the plasma. However, since the desired region of current drive is in the outer radius of the plasma, the wave will deposit its energy into the electrons before it reaches a mode conversion point. The addition of a 10% density of fast electrons does not change these accessibility conditions.

By using the imaginary parts of the warm plasma dispersion relation, previous studies [9] determined that a region of ideal Landau damping would be reached when $v_{ph} / v_{tle} \approx 2.5$. Direct determination of Landau damping rates by using a technique developed by Stix [19] confirms this. By adapting the

hot plasma dispersion relation to accommodate 10% fast electrons, the required value of $n_{\parallel edge}$ is estimated to decrease by almost 20%.

Figures (5) and (6) show ray trajectories and power deposition profiles obtained using the required value of $n_{\parallel edge}$ in an RFP-adapted version of the Brambilla ray-tracing program [10]. Estimated values of $n_{\parallel edge}$ for the full density scan of RFX are presented in Table I. These results are encouraging and support the use of lower hybrid current drive as a method of fluctuation suppression and improved confinement in an RFP.

Finally, we note that Shiina, *et al.* [21] have expanded their RF current drive studies for the large aspect ratio RFP to encompass Whistler and electron cyclotron waves in addition to fast and lower hybrid waves. They have concluded that, although the fast wave may be a useful candidate for full current drive, the lower hybrid wave would be effective for the purpose of driving current in the outer regions of the RFP in order to reverse the toroidal field and improve energy confinement time.

ACKNOWLEDGEMENTS

This work is supported by the U.S. Department of Energy grant numbers DE-FG02-85ER53212 and DE-FG02-85ER53198 and contract number DE-AC03-89ER51114.

REFERENCES

1. TAYLOR, J.B., Phys. Rev. Lett. **33**, 1139 (1974).

2. ALMAGRI, A., et al., Phys. Fluids B **4**, 4080 (1992).

3. FIKSEL, G., et al., Phys. Rev. Lett. **72**, 1028 (1994).

4. STONEKING, M., et al., Phys. Rev. Lett. **73**, 549 (1994).

5. HO, Y.L., Nuc. Fusion **31**, 341 (1991).

6. SARFF, J.S., et al., Phys. Rev. Lett. **72**, 3670 (1994).

7. SHIINA, S., et al., Nuc. Fusion **34**, 1473 (1994).

8. ISHII, H., et al., in *Proceedings of the Twentieth European Physical Society Conference on Controlled Fusion and Plasma Physics, 1993*, Lisboa (European Physical Society), Vol. 17C, p. 495.

9. UCHIMOTO, E., et al., Phys. Plasmas **1**, 3517 (1994).

10. BRAMBILLA, M., Comp. Phys. Rep. **4**, 73 (1986).

11. SCHNACK, D.D., et al., J. Comp. Physics **70**, 330 (1987).

12. MALESANI, G., in *Proceedings of the International School of Plasma Physics Workshop on Physics of Mirrors, Reversed Field Pinches, and Compact Tori, 1987*, Varenna (Società Italiana di Fisica, Bologna), Vol. 1, p. 331.

13. DEXTER, R.N., et al., Fusion Technol. **19**, 131 (1991).

14. HOKIN, S.A., et al., Nuc. Fusion **34**, 1447 (1994).

15. ORTOLANI, S., Plasma Phys. and Cont. Fusion **34**, 1903 (1992).

16. STONEKING, M.R., Fast electron generation and transport in a turbulent, magnetized plasma, Ph.D. thesis, University of Wisconsin - Madison (1994).

17. SWANSON, D.G., Plasma Waves, Academic Press, Inc., Boston (1989).

18. UCHIMOTO, E., et al., Bull. Am. Phys. Soc. **38**, 1979 (1993).

19. STIX, T.H., Nuc. Fusion **15**, 737 (1975).

20. HOKIN, S.A., et al., in *Proceedings of the 14th International Conference on Plasma Physics and Controlled Nuclear Fusion, 1992*, Wurzburg (International Atomic Energy Agency, Vienna, 1993), p. 539.

21. SHIINA, S., et al., Fus. Eng. and Des. **26**, 259 (1995).

CAPTIONS

Table I: Temperature and densities for RFX in a conventional density scan. In the first column, I/N is the toroidal current over $N = \pi a^2 \langle n \rangle$ in which a is the minor radius and $\langle n \rangle$ is the volume averaged density. Predicted $n_{//edge}$ are included.

Figure 1: Contour plot of $n_\perp^2 = 0$. The path of the wave through the plasma has been marked by 'x' and labeled with the corresponding r/a value. The dashed curve shows the region of the resonance between the wave parallel phase velocity and the electron parallel thermal velocity. The dotted curve represents the location of the cutoff derived from cold plasma theory and expressed in Eq. (8).

Figure 2: Plots of values of $n_\perp^2$ for the slow and fast wave as density increases for selected values of $n_{//}$ in RFX. The extra path at the mode conversion point is an evanescent mode inside the cutoff.

Figure 3: Contours of $v_{ph} / v_{t//e}$ over parallel index of refraction and temperature. Prior analysis predicted that optimal Landau damping occurs where $v_{ph}/v_{t//e} \approx 2.5$. The path of the ray is marked by 'x' and labeled with the corresponding value of r/a. Here, the ray is located for ideal Landau damping in the region $r/a \approx 0.7$.

Figure 4: Landau damping rate (solid) versus Δt (dotted) as a function of r/a for the cases of $n_{//edge} = 4.5$ to $n_{//edge} = 6.0$. The point of intersection of the two curves marks the region of ideal Landau damping. In order to drive current at $r/a \approx 0.70$, $4.5 > n_{//edge} > 5.5$ appears to be appropriate.

Figure 5: Ray trajectory in a constant toroidal angle plane for RFX where $n_{//edge} \approx 5.5$. The ray is launched at the wall and makes slightly less than two poloidal transits before being completely absorbed by the plasma. It should be noted here that the toroidal shear has been suppressed for these calculations.

Figure 6: Power deposition profile for the lower hybrid wave launched into RFX with $n_{//edge} = 5.5$. The spike located at $\psi \approx 0.70$ (ψ is a flux surface coordinate analogous to r/a which is equal to 1.0 at the plasma edge) is indicative of a relatively large amount of power to the electrons at this point and, therefore, of current driven in this region. Power delivered to the ions was negligible.

Figure 7: Ray trajectory in a constant toroidal angle plane for RFX where $n_{//edge}$ is allowed to vary. a) The parallel index of refraction is below the cutoff for the edge density of RFX and the wave is evanescent. b) The parallel index of refraction allows the wave to enter the plasma edge, but not to propagate further. The wave is a surface wave. c) The wave makes just over three poloidal transits for $n_{//edge} = 4.0$. d) The wave damps out within one poloidal transit for $n_{//edge} = 8.0$. As in Figure 5, toroidal shear has been suppressed for these calculations.

Figure 8: Power deposition profiles for the cases discussed in Figure 7. Note that the electrons receive maximum power at c) $\psi = 0.60$ for $n_{//edge} = 4.0$ and d) $\psi = 0.85$ for $n_{//edge} = 8.0$.

Figure 9: As in Figure 1, but for an RFX plasma with 10% hot electrons. Note that the thermal resonance has shifted to lower $n_{//}$.

Figure 10: As in Figure 4 but for an RFX plasma with 10% fast electrons. The ideal damping points for each figure have shifted toward the edge of the plasma. To maintain optimal damping, this corresponds to a 20% increase in the wave's phase velocity at the edge of the plasma.

Table I

I/N (x 10^{-14} A·m)	n (x 10^{13} cm^{-3})	T_e (eV)	n_{lledge}
2	15.6	600	5.7 - 7.0
4	7.8	790	5.0 - 6.2
6	5.2	940	4.5 - 5.7
8	3.8	1060	4.4 - 5.4
10	3.1	1140	4.2 - 5.2

TABLE I

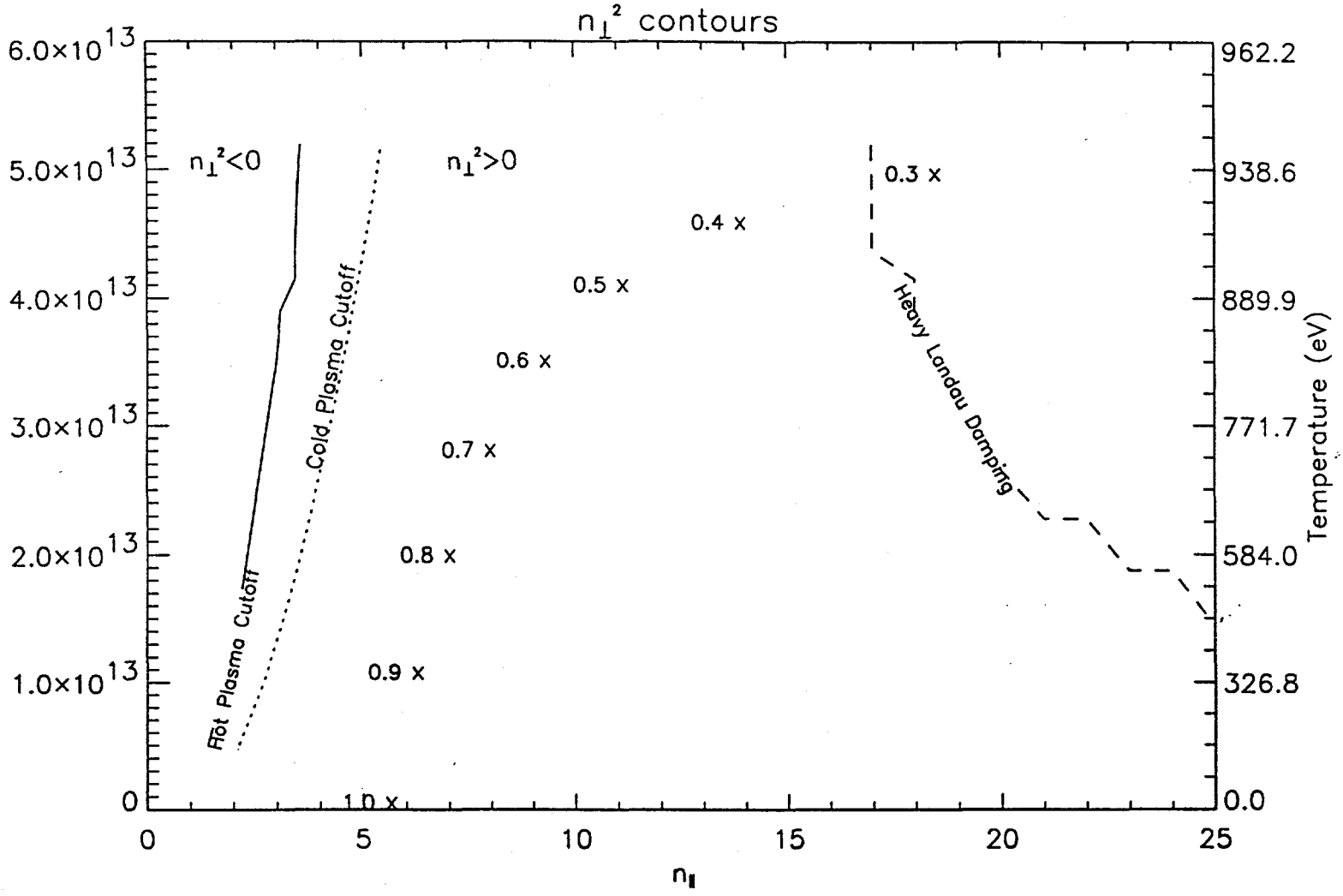
$n_\perp^2$ contours
$n_\perp^2<0$
$n_\perp^2>0$
Hot Plasma Cutoff
Cold Plasma Cutoff
Heavy Landau Damping
0.3 x
0.4 x
0.5 x
0.6 x
0.7 x
0.8 x
0.9 x
1.0 x
6.0×10^{13}
5.0×10^{13}
4.0×10^{13}
3.0×10^{13}
2.0×10^{13}
1.0×10^{13}
0
962.2
938.6
889.9
771.7
584.0
326.8
0.0
Temperature (eV)
0
5
10
15
20
25
$n_\parallel$

FIGURE 1

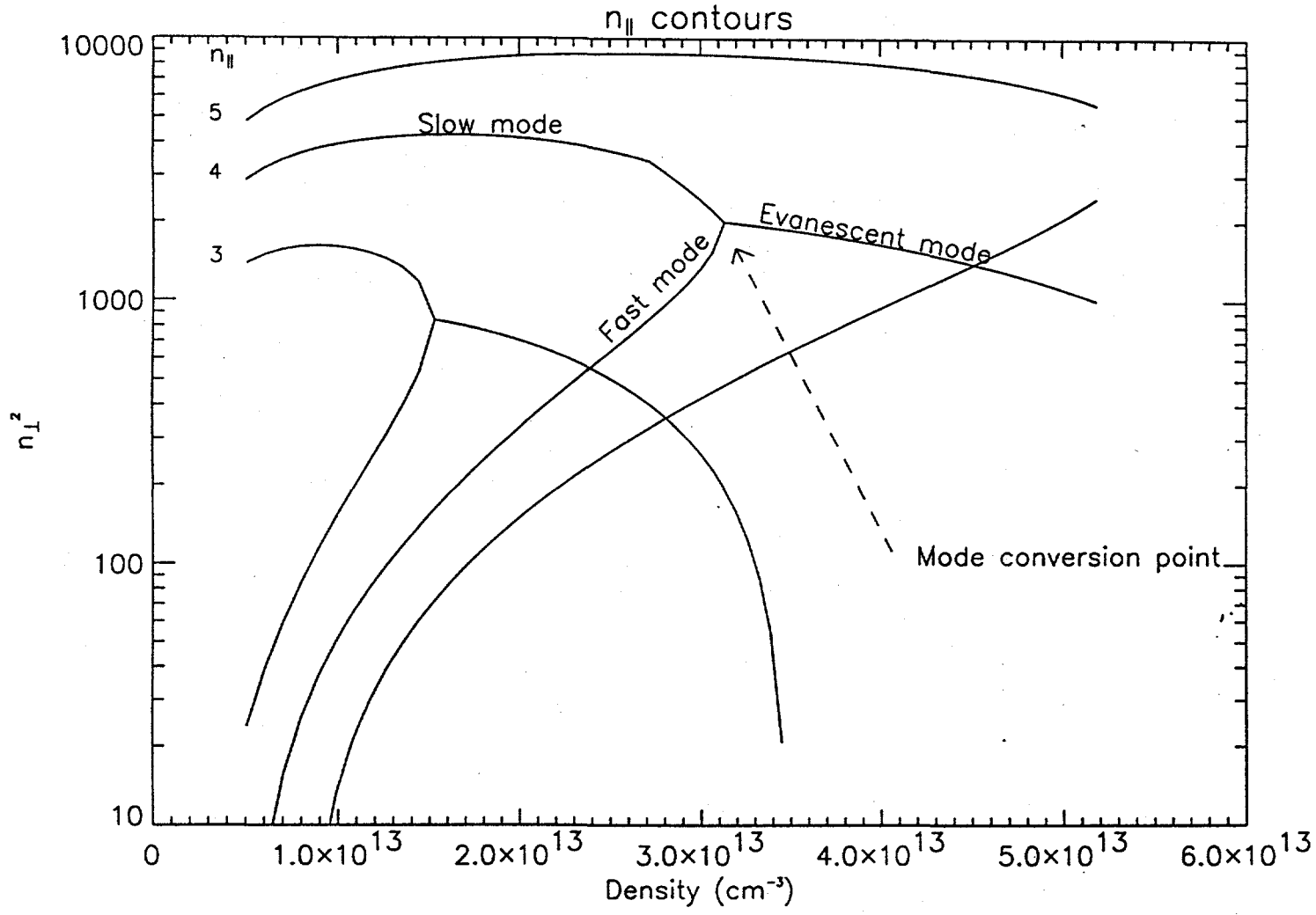
$n_\parallel$ contours
10000
1000
100
10
$n_\perp^2$
$n_\parallel$
5
4
3
Slow mode
Fast mode
Evanescent mode
Mode conversion point
0
1.0×10^13
2.0×10^13
3.0×10^13
4.0×10^13
5.0×10^13
6.0×10^13
Density (cm^-3)

FIGURE 2

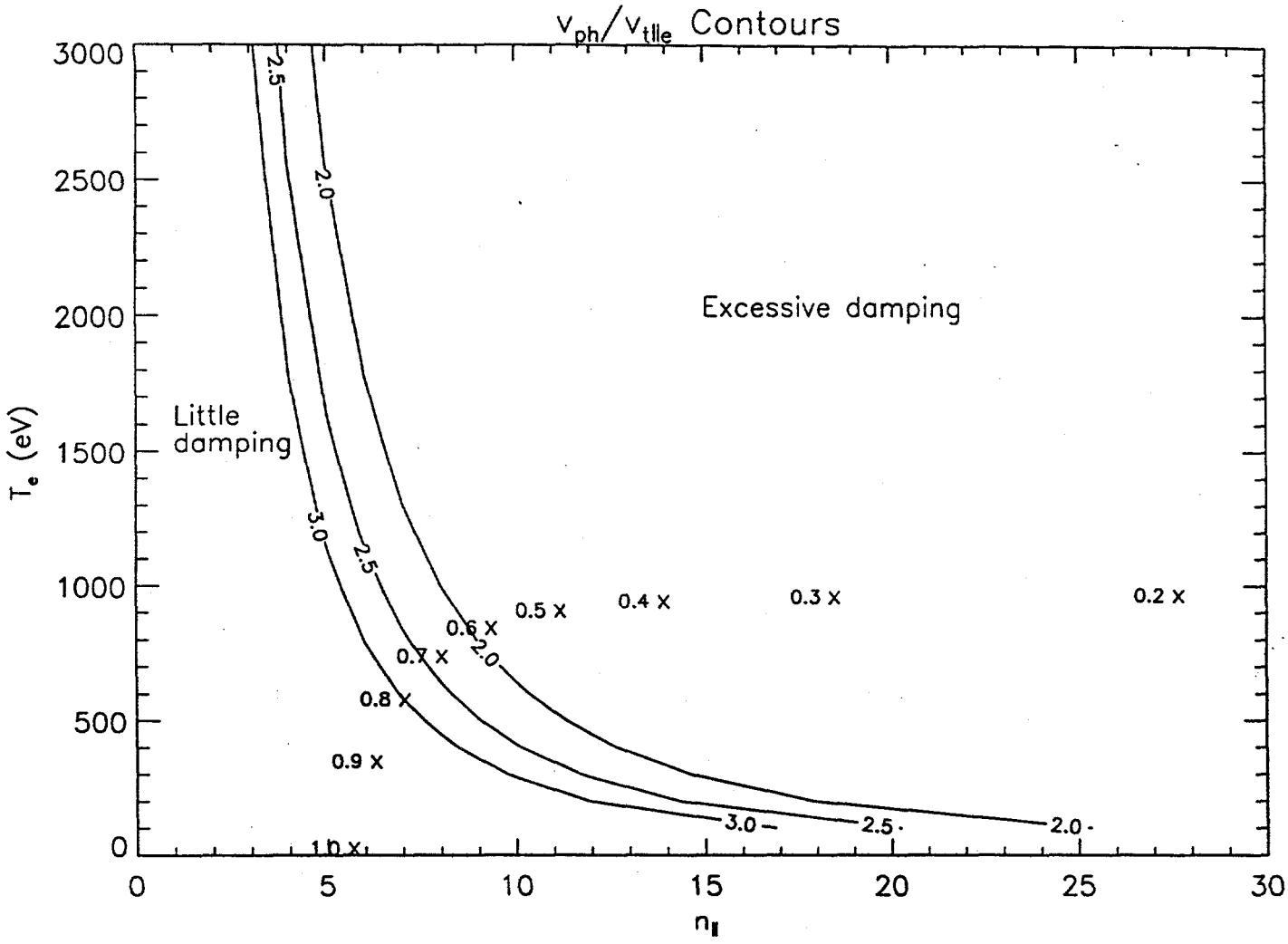
v_{ph}/v_{tle} Contours
Excessive damping
Little damping
2.5
2.0
3.0
2.5
2.0
0.5 X
0.4 X
0.3 X
0.2 X
0.6 X
0.7 X
0.8 X
0.9 X
1.0 X
3.0
2.5
2.0
T_e (eV)
$n_\parallel$
0
500
1000
1500
2000
2500
3000
0
5
10
15
20
25
30

FIGURE 3

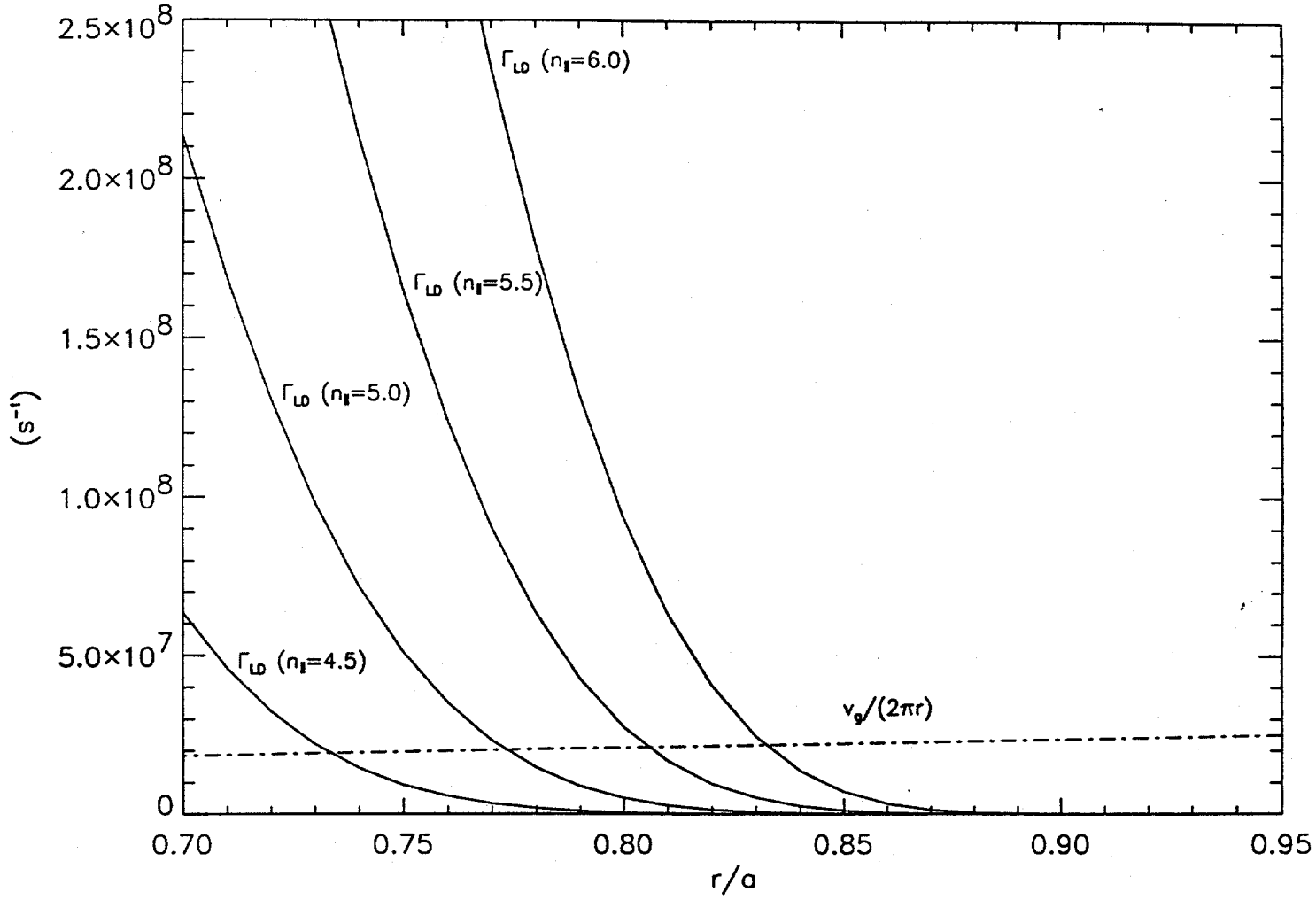
2.5×10^8
2.0×10^8
1.5×10^8
1.0×10^8
5.0×10^7
0
(s^-1)
Γ_LD (n_∥=6.0)
Γ_LD (n_∥=5.5)
Γ_LD (n_∥=5.0)
Γ_LD (n_∥=4.5)
v_g/(2πr)
0.70
0.75
0.80
0.85
0.90
0.95
r/a

FIGURE 4

Ray Trajectory in the Poloidal Plane

$n_{\|edge} = 5.5$

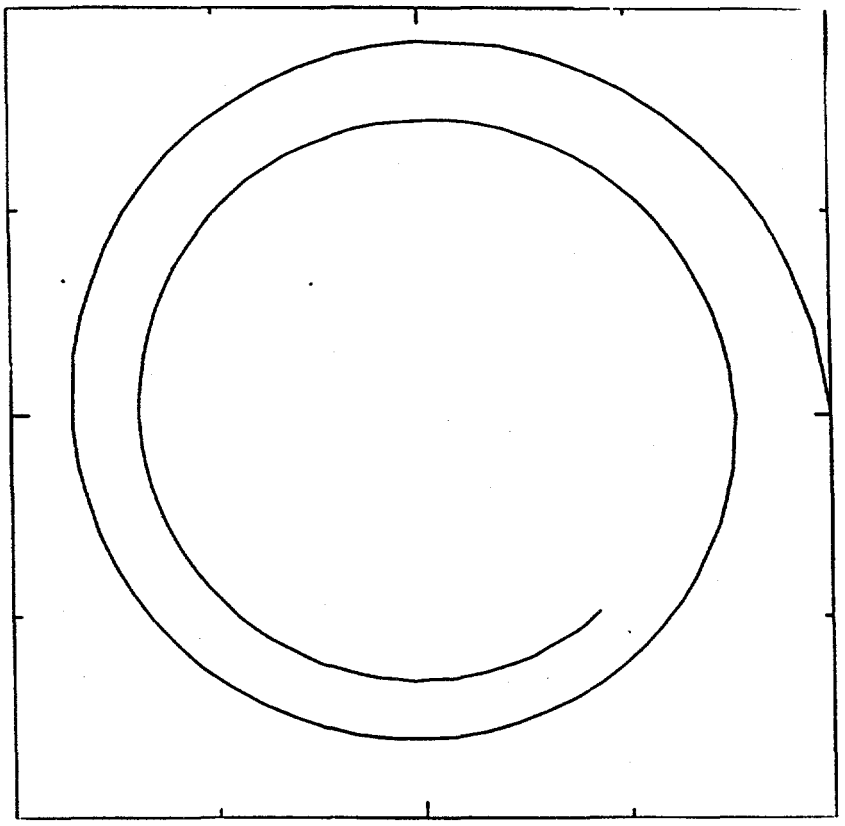

FIGURE 5

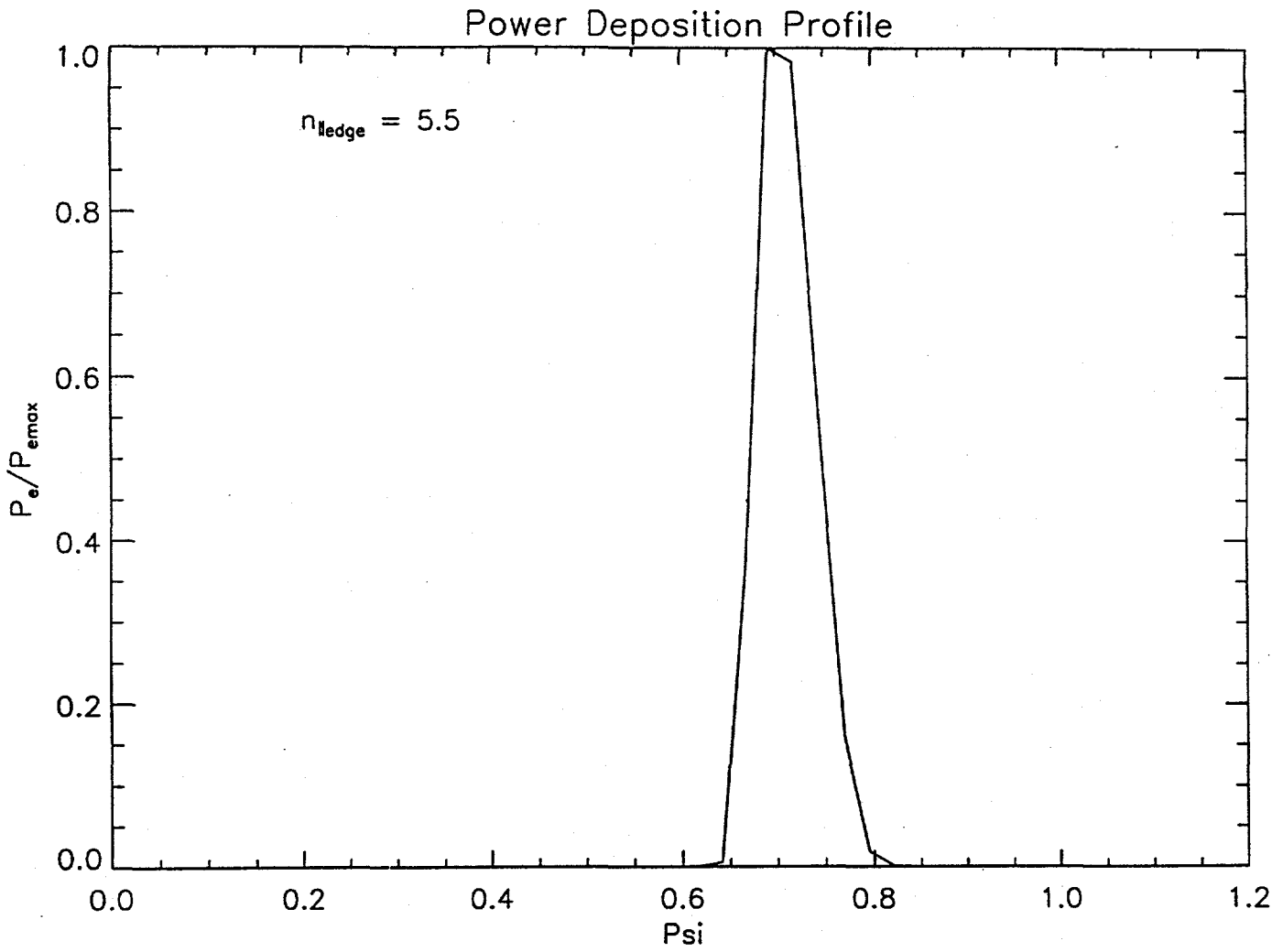
Power Deposition Profile
$n_{\parallel edge}$ = 5.5
P_e/P_{emax}
Psi
1.0
0.8
0.6
0.4
0.2
0.0
0.0
0.2
0.4
0.6
0.8
1.0
1.2

FIGURE 6

Ray Trajectory in the Poloidal Plane

a) $n_{//edge} = 2.4$

Wave is evanescent.

b) $n_{//edge} = 2.6$

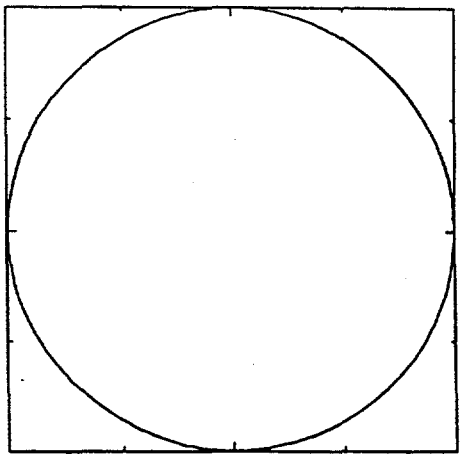

c) $n_{//edge} = 4.0$

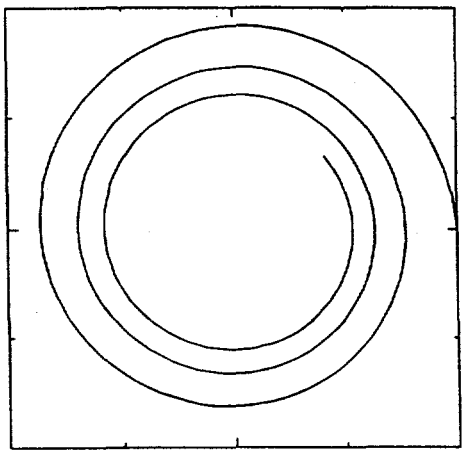

d) $n_{//edge} = 8.0$

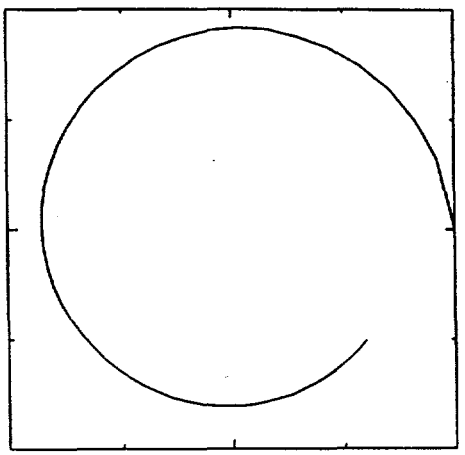

FIGURE 7

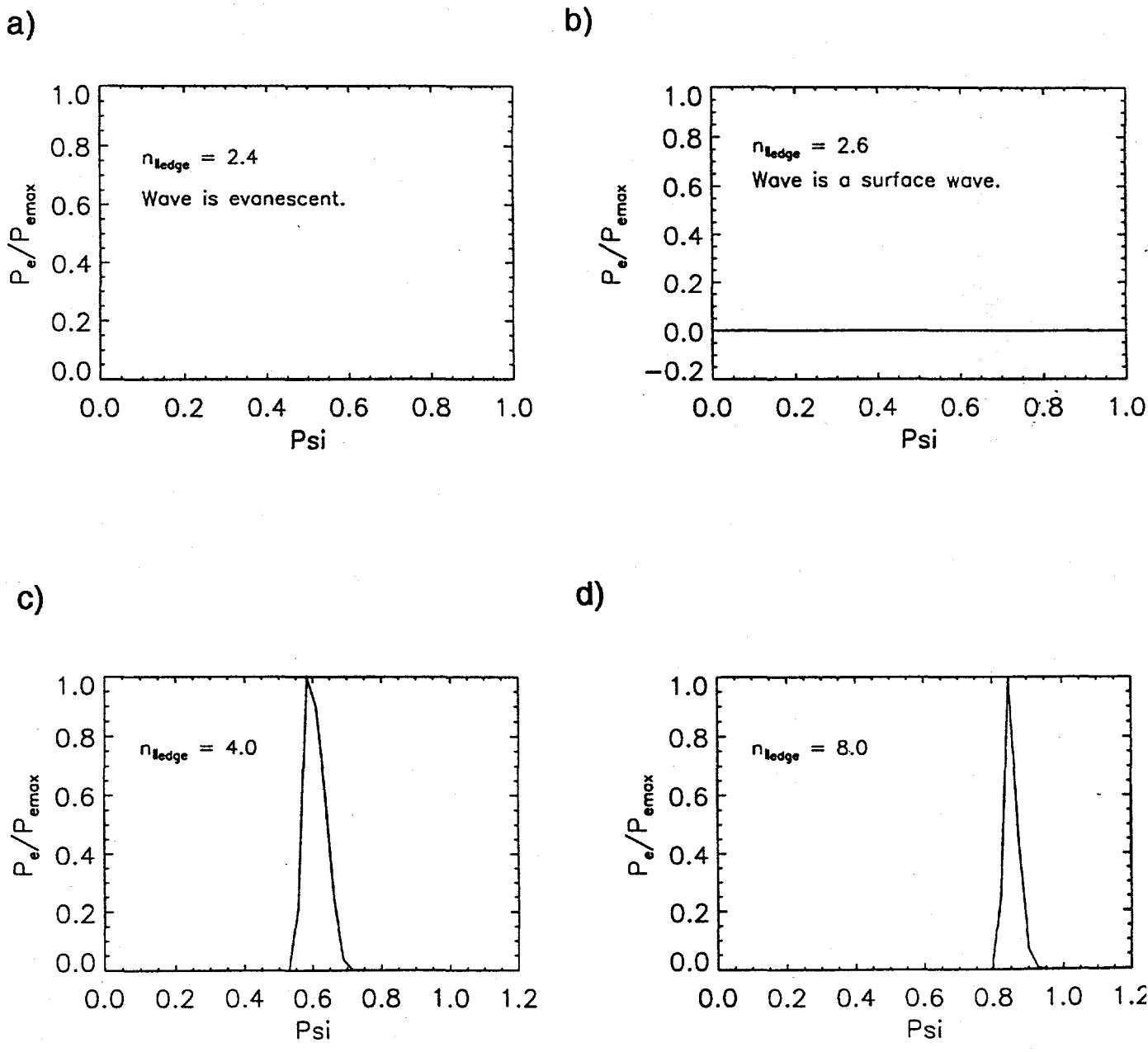
a)
b)
c)
d)
P_e/P_{emax}
Psi
n_{iledge} = 2.4
Wave is evanescent.
n_{iledge} = 2.6
Wave is a surface wave.
n_{iledge} = 4.0
n_{iledge} = 8.0

FIGURE 8

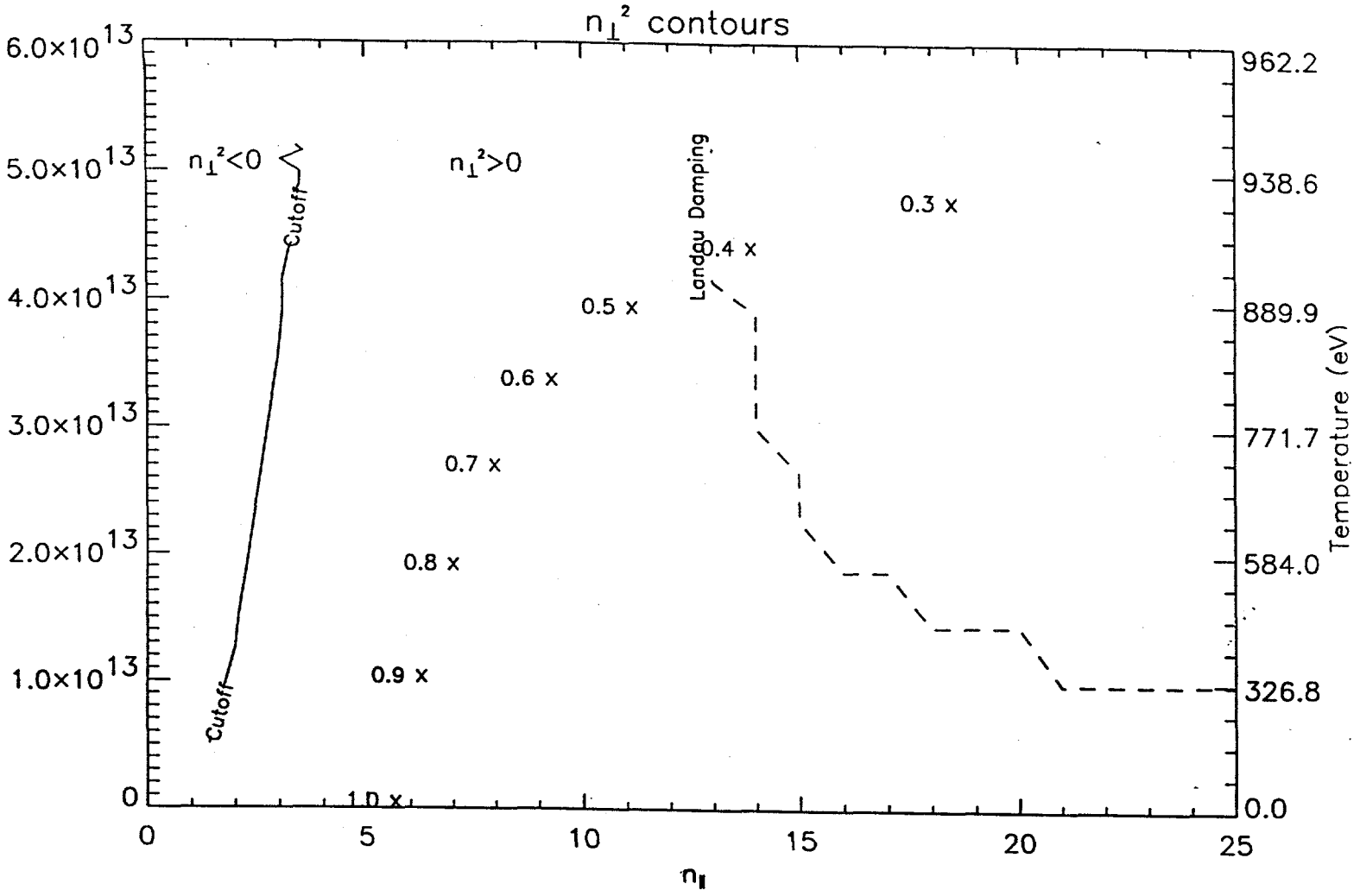
$n_\perp^2$ contours
$n_\perp^2<0$
$n_\perp^2>0$
Cutoff
Cutoff
Landau Damping
0.3 x
0.4 x
0.5 x
0.6 x
0.7 x
0.8 x
0.9 x
1.0 x
6.0×10^{13}
5.0×10^{13}
4.0×10^{13}
3.0×10^{13}
2.0×10^{13}
1.0×10^{13}
0
962.2
938.6
889.9
771.7
584.0
326.8
0.0
Temperature (eV)
0
5
10
15
20
25
$n_\parallel$

FIGURE 9

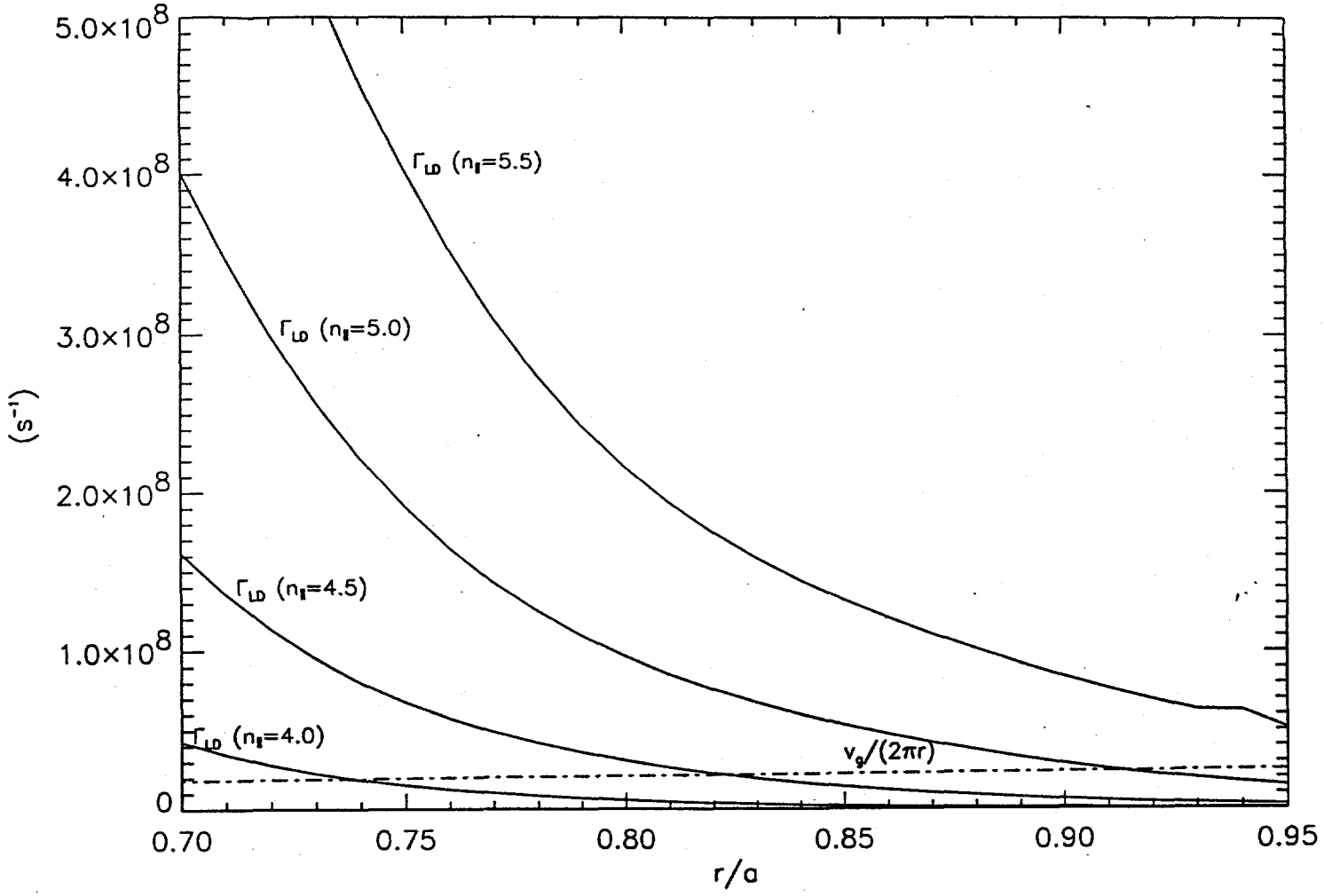
5.0×10^8
4.0×10^8
3.0×10^8
2.0×10^8
1.0×10^8
0
(s^-1)
Γ_LD (n_∥=5.5)
Γ_LD (n_∥=5.0)
Γ_LD (n_∥=4.5)
Γ_LD (n_∥=4.0)
v_φ/(2πr)
0.70
0.75
0.80
0.85
0.90
0.95
r/a

FIGURE 10

EXTERNAL DISTRIBUTION IN ADDITION TO UC-20

S.N. Rasband, Brigham Young University
R.A. Moyer, General Atomics
J.B. Taylor, Institute for Fusion Studies, The University of Texas at Austin
E. Uchimoto, University of Montana
F.W. Perkins, PPPL
O. Ishihara, Texas Technical University
M.A. Abdou, University of California, Los Angeles
R.W. Conn, University of California, Los Angeles
P.E. Vandenplas, Association Euratom-Etat Belge, Belgium
Centro Brasileiro de Pesquisas Firicas, Brazil
P. Sakanaka, Institute de Fisica-Unicamp, Brazil
Mme. Monique Bex, GANIL, France
J. Radet, CEN/CADARACHE, France
University of Ioannina, Greece
R. Andreani, Associazione EURATOM-ENEA sulla Fusione, Italy
Biblioteca, Istituto Gas Ionizzati, EURATON-ENEA-CNR Association, Italy
Plasma section, Energy Fundamentals Division Electrotechnical Laboratory, Japan
Y. Kondoh, Gunma University, Kiryu, Gunma, Japan
H. Toyama, University of Tokyo, Japan
Z. Yoshida. University of Tokyo, Japan
FOM-Instituut voor Plasmafysica "Rijnhuizen," The Netherlands
Z. Ning, Academia Sinica, Peoples Republic of China
P. Yang, Shandong University, Peoples Republic of China
S. Zhu, University of Science & Technology of China, People's Republic of China
I.N. Bogatu, Institute of Atomic Physics, Romania
M.J. Alport, University of Natal, Durban, South Africa
R. Storer, The Flinders University of South Australia, South Australia
B. Lehnert, Royal Institute of Technology, Sweden
Librarian, CRPP, Ecole Polytechnique Federale de Lausanne, Switzerland
B. Alper, Culham Laboratory, UK
A. Newton, UK

2 for Chicago Operations Office
5 for individuals in Washington Offices

INTERNAL DISTRIBUTION IN ADDITION TO UC-20
80 for local group and file